Proposal for the J-PARC 30-GeV Proton Synchrotron

Systematic investigations of the light kaonic nuclei
– produced via the in-flight $^4\mathrm{He}(K^-, N)$ reactions –

ver. June 16, 2020

H. Asano K. Itahashi, M. Iwasaki, Y. Ma, R. Murayama, H. Outa, F. Sakuma[*],
T. Yamaga

RIKEN Cluster for Pioneering Research, RIKEN, Saitama, 351-0198, Japan

K. Inoue, S. Kawasaki, H. Noumi, K. Shirotori

*Research Center for Nuclear Physics (RCNP), Osaka University, Osaka, 567-0047,
Japan*

H. Ohnishi, Y. Sada, C. Yoshida

*Research Center for Electron Photon Science (ELPH), Tohoku University, Sendai,
982-0826, Japan*

T. Hashimoto

Japan Atomic Energy Agency (JAEA), Ibaraki 319-1195, Japan

M. Iio, S. Ishimoto, K. Ozawa, S. Suzuki

High Energy Accelerator Research Organization (KEK), Ibaraki, 305-0801, Japan

T. Akaishi

Department of Physics, Osaka University, Osaka, 560-0043, Japan

T. Nagae

Department of Physics, Kyoto University, Kyoto, 606-8502, Japan

M. Bazzi, A. Clozza, C. Curceanu, C. Guaraldo, M. Iliescu, M. Miliucci, A. Scordo,
D. Sirghi, F. Sirghi

Laboratori Nazionali di Frascati dell' INFN, I-00044 Frascati, Italy

P. Buehler, M. Simon, E. Widmann, J. Zmeskal

Stefan-Meyer-Institut für subatomare Physik, A-1090 Vienna, Austria

---

[*]Spokesperson, E-mail: sakuma@ribf.riken.jp

Abstract

We propose a series of experimental programs for the systematic investigation of the kaon-nuclear bound states in light nuclei, from the "$\bar{K}N$" (=$\Lambda(1405)$) to "$\bar{K}NNNN$". By this series of experimental programs, we provide the whole picture of the kaon-nuclear bound states. We will deduce the direct information of the interplay between spontaneous and explicit chiral symmetry braking in the nuclear matter from the measurments of the property changes depending on the mass number.

The kaonic nuclei can be produced via the in-flight (K^-, N) reactions using the world's highest low-momentum DC kaon beam available at J-PARC. The simplest kaonic nuclear system of the "K^-pp" state has been observed in the $^3\mathrm{He}(K^-, \Lambda p)n$ measurement at the predecessor experiment J-PARC E15. The observed much deeper binding energy, compared to that of normal nuclei, is partially supporting theoretical calculations based on the strongly attractive $\bar{K}N$ interaction. For further studies of the kaonic nuclei, we need to add nucleons to the target nuclei, *i.e.*, the A dependence of the kaonic nuclei should be revealed. However, with large target nuclei, an experiment becomes extremely difficult to handle number of particles in the final state and to determine possible reaction channels. Although we wish to reach the kaonic nuclei with $^4\mathrm{He}$ core ($A = 4$) which would be compact and tightly bound system, we need to have an outlook of the experimental approach. In this proposal, we discuss the $\bar{K}NNN$ ($A = 3$) system as a bridge to the $A = 4$ system. The promising decay channels to be detected are non-mesonic decays of the $K^-ppn \rightarrow \Lambda d$ and Λpn channels in the $^4\mathrm{He}(K^-, \Lambda d/\Lambda pn)n$ measurements.

To realize the systematic measurements, a large acceptance spectrometer capable of neutral particle detection and efficiently usage of the high intensity kaon beam are mandatory. For this purpose, we are planning to construct a totally new spectrometer system, *i.e.*, a 4π cylindrical detector system (CDS). The new spectrometer drastically improves the acceptance resulting efficiently particle detection in the final state, and enables us to specify the reaction channel in unambiguous manner. In addition, we propose to shorten the K1.8BR beamline to compensate the kaon decay before the target.

Summary of the proposed experiment

beamline:	K1.8BR
Primary beam:	30 GeV, 90kW (5.2 s spill interval)
Secondary beam:	1.0 GeV/c K^-
Beam intensity:	3.2×10^5 on target per pulse
Reaction:	in-flight (K^-, N)
Detectors:	modified K1.8BR beamline spectrometer, and
	new cylindrical detector system
Target:	Liquid ^{4}He
Beam time:	1 week for detector commissioning,
	1 week for performance study with H$_2$ target, and
	3 weeks for the physics run with ^{4}He target
Estimated yield:	1.9×10^4 $K^- ppn \rightarrow \Lambda d$, and
	2.8×10^3 $K^- ppn \rightarrow \Lambda pn$

1 Introduction

The study of the $\bar{K}N$ interaction is one of the most important subjects to understand meson-baryon interactions in low energy quantum chromodynamics (QCD). Extensive measurements of anti-kaonic hydrogen atom [1–3] and low-energy $\bar{K}N$ scattering [4] have revealed the strongly attractive $\bar{K}N$ interaction in the isospin I = 0 channel. As a consequence, possible existence of deeply-bound kaonic nuclear states has been widely discussed [5–24].

Among the kaonic nuclear states, the $\bar{K}NN$ system with $I = 1/2$ and $J^P = 0^-$ (symbolically denoted as "K^-pp") is of special interest because it is the lightest $S = -1$ $\bar{K}$ nucleus and whose existence is supported by many theoretical works today. Over the past nearly 20 years, however, the existence of the "K^-pp" was not been established despite of many experimental efforts. Several groups reported an observation of a "K^-pp" candidate with the binding energy of around 100 MeV, in experiments which measured non-mesonic decay branches of Λp and/or $\Sigma^0 p$ in different reactions [25–27]. On the other hand, there also are reports concluding that the reactions can be understood without the inclusion of a bound state [28–31]. Recently, the J-PARC E15 experiment pinned down the existence of the "K^-pp" bound state by using the simplest reaction of in-flight $^3\text{He}(K^-, N)$ [32–34]. A distinct peak structure was observed well below the mass threshold of $K^- + p + p$ in the Λp invariant-mass spectrum, obtained from the $^3\text{He}(K^-, \Lambda p)n$ measurement. The simplest and natural interpretation of this peak is a kaonic-nuclear bound-state, "K^-pp". This result is experimentally solid as against the previously reported results, thus the existence of the "K^-pp" bound state is experimentally clarified at last.

To obtain further understanding of the kaonic nuclei, the system size dependence of those properties are of importance. There are several theoretical calculations of such dependence with the different $\bar{K}N$ interaction model. Thus the systematic studies of the kaonic nuclei would reveal the $\bar{K}N$ interaction below the mass threshold by comparing with those theoretical calculations. The state of the kaonic nuclei is predicted to be compact due to the strong attraction of the $\bar{K}N$, which indicates that the high-density nuclear matter is realized in kaonic nuclei. Therefore, the determinations of the form factor and decay-branching ratio of the kaonic nuclei are also mandatory to shed light on the internal structure. The spin and parity measurements are of course crucial to understand whether or not the observed "kaonic nuclei" are the theoretically predicted objects. For the determination, we need decay-branching measurements with full solid angle coverage.

At the K1.8BR beamline, a series of experimental programs have been planned to aim a systematic investigation of the kaon-nuclear bound systems in light nuclei, *i.e.*, from the "$\bar{K}N$" $(=\Lambda(1405))$ to "$\bar{K}NNN$". The experimental series is realized by using the world's highest intensity of low-momentum kaon beam at J-PARC. The programs mainly consist of:

- Precise measurement of the $\Lambda(1405)$ state in large momentum transfer region via

the $d(K^-, n)$ reaction,

- Investigation of the spin and parity of the $\bar{K}NN$ state via the $^3\text{He}(K^-, N)$ reactions,

- Search for the $\bar{K}NNN$ states via the $^4\text{He}(K^-, N)$ reactions, and,

- Advanced search for the $\bar{K}NNNN$ states via the $^6\text{Li}(K^-, d)$ reaction.

Furthermore, in the future, we plan to explore $S = -2$ kaonic nuclei such as the theoretically predicted K^-K^-pp state, which would be much higher dense matter compared to the normal kaonic nuclei with $S = -1$. One possible way for the measurement at J-PARC is:

- Search for the $\bar{K}\bar{K}NN$ states via the $\bar{p} + {}^3\text{He}$ annihilation,

however, whose production cross section is expected to be quite small – roughly one-thousandth of that of the normal kaonic nuclei.

For the systematic and precise measurements, we are planing to construct a totally new 4π spectrometer to measure all particles involved in the reactions and to reconstruct its formation and decay exclusively. The spectrometer is designed to keep high versatility that all the experiments can be performed by changing the target materials. In addition, to use the high-intensity kaon beam further efficiently, we propose modification of the existing K1.8BR beam-line by shortening the length of the beam line, which can be realized by removing the most downstream dipole magnet of D5.

In the proposal, we focus on the experiment to search for the $\bar{K}NNN$ bound state as the first stepping stone to accomplish the systematic investigation of the light kaonic nuclei. Besides this proposal, we are now preparing the other new proposal for the precise investigation of the $\bar{K}NN$ system using ^3He target, in which we attempt to determine the spin of the system by measuring the polarization of decay particles. The other challenging experiments – $\Lambda(1405)$ production in high momentum transfer region and the $\bar{K}NNNN/\bar{K}\bar{K}NN$ bound state search – will also be proposed in the near future.

We introduce an overview of the "K^-pp" measurement at the E15 experiment in the rest of this section to show what we have learned from the modern experimental investigation dedicated to the kaonic nuclei. Then we show the details of the proposed experiment focusing on the $\bar{K}NNN$ search in Sec.2 and subsequent sections.
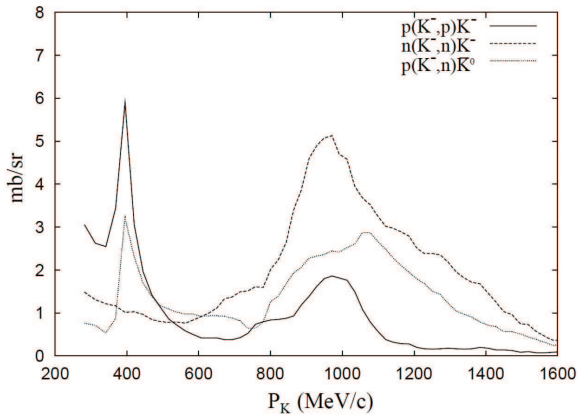
Figure 1: Cross sections of the $\bar{K}N \to \bar{K}N$ reactions at $\theta_n = 0$ (neutron forward / kaon backward) [35].

1.1   Results of the E15 Experiment

We conducted an experimental investigation of the "K^-pp" bound state using the simplest $\bar{K}$ induced reaction of $K^- + {}^3$He via the nucleon knock-out reactions $\bar{K}N \to$ '$\bar{K}$'N followed by two nucleon absorption of '$\bar{K}$'$+NN \to$ "K^-pp". In the experiment, we used the kaon momentum of 1 GeV/c where the $\bar{K}N \to \bar{K}N$ reactions have the maximum cross section as shown in Fig 1. The recoiled kaon '$\bar{K}$' at a momentum q behaves as a 'off-shell particle' (total energy can be lower than its intrinsic mass) within a time range what the uncertainty principle allows, where the momentum transfer q is defined between the incident kaon and the outgoing neutron in the laboratory frame $q = |\boldsymbol{p}_{K^-}^{lab} - \boldsymbol{p}_n^{lab}|$. In the reaction, we utilized this low-momentum back-scattered kaon as a 'off-shell kaon' source and residual spectator nucleons NN as an 'actual target' to form a "K^-pp" state, whose energy below their intrinsic mass of $M(Kpp)$ ($= m_K + 2m_N = 2.37$ GeV/c^2). In this way, we can access the bound energy region, where it is not accessible in other reaction.

   With the Λpn final states, we observed a kinematic anomaly in the Λp invariant mass near the mass threshold of $M(Kpp)$ at the lower momentum transfer region [32–34]. As shown in Fig. 2 (left), we confirmed the existence of the bound state below the mass threshold of $M(Kpp)$, whose mass centroid is independent on q, at as deep as the binding energy of ~ 50 MeV [34]. The momentum transfer q naturally prefers lower momentum for the bound state formation, but the event concentration can not be seen in the larger q region more than ~ 600 MeV/c. These facts indicate the formation of deeply bound and spatially compact object. The back-scattered 'on-shell' kaon, whose total kaon energy is above its intrinsic mass, can also be absorbed by the spectator nucleons without forming a bound state. The kinematical centroid of such quasi-free absorption process is plotted in the figure, denoted as QF_K. Along the line, there are two event concentration points at $\theta_n = 0$ and $\theta_n = \pi$, but both are well separated from

6
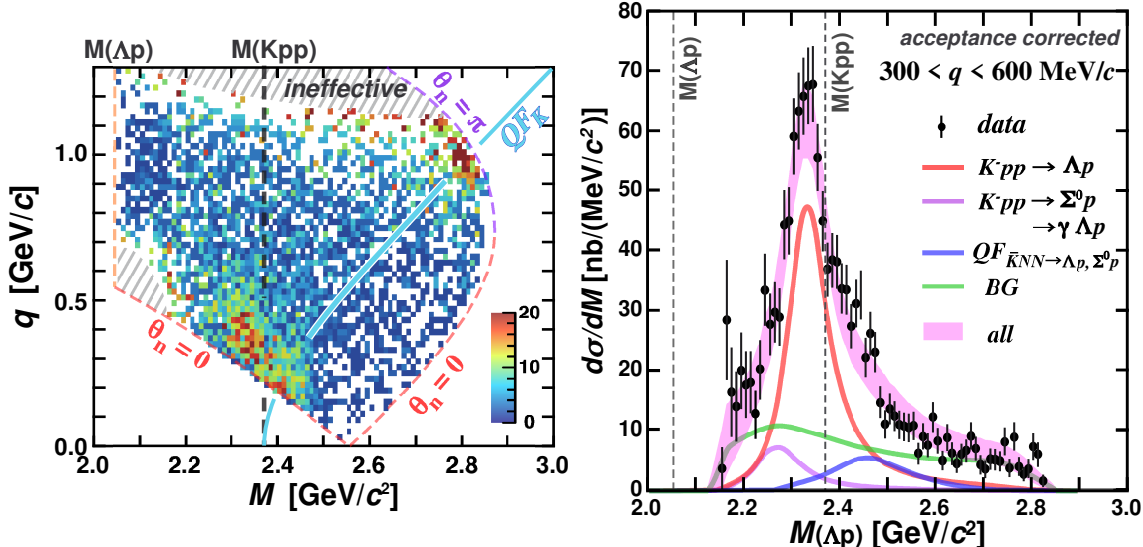
Figure 2: (left) Efficiency and acceptance corrected data over M (Λp invariant mass) and q (momentum transfer). (right) The Λp invariant mass in the region of $0.3 < q < 0.6$ MeV/c.

the region of interest. Figure 2 (right) shows the acceptance and efficiency corrected Λp invariant mass in the region of $0.3 < q < 0.6$ GeV/c, where the "$K^- pp$" bound state is clearly separated from the quasi-free absorption process. A clear peak originated from the "$K^- pp$" can be seen below $M(Kpp)$, whose binding energy reaches to ~ 50 MeV. We also excluded all the possible processes which may form a spurious structure in the Λp invariant mass spectrum. Thus the simplest and natural interpretation is a kaon-nuclear bound state "$K^- pp$".

Then a question arises whether or not the "$K^- p$" bound state is also produced in the same $K^- + {}^3$He reaction. The $\Lambda(1405)$ state with $I = 0$, which locates slightly below the $\bar{K}N$ mass threshold and decays into $\pi\Sigma$, is theoretically considered as a quasi-bound state of $\bar{K}N$ in the $I = 0$ as supported by lattice QCD calculation [36]. Hence, an investigation of the $\Lambda(1405)$ production in the $K^- + {}^3$He reaction is crucial together with the "$K^- pp$" production. Indeed, the production mechanism of the $\bar{K}NN$ system is assumed with a $\Lambda(1405) + N \to \bar{K}NN$ doorway process in theoretical models [37]. From our recent analysis of an exclusive measurement of the $\Lambda(1405)$ state produced in the reaction $K^- + {}^3$He $\to Y^{*0} + p + n$, an important hint of the production mechanism of the "$K^- pp$" bound state has been obtained.

Figure 3 (left) shows the invariant-mass spectrum of $\pi^\pm\Sigma^\mp$ in the $\pi^\pm\Sigma^\mp pn$ final states. The $\Lambda(1405)$ state is clearly identified, whose cross section of ~ 200 μb has been obtained by simple Breit-Wigner fit. By comparing the obtained "$K^- pp$" $\to \Lambda p$ cross section of ~ 10 μb, the production of the $\Lambda(1405)$ is ~ 10 times large. Then the $\Lambda(1405)pn$ final state is selected with the region below the $\Lambda(1520)$ region, which can be compared to Λpn final state. The $\pi^\pm\Sigma^\mp p$ invariant-mass spectrum in the $\Lambda(1405)$

7
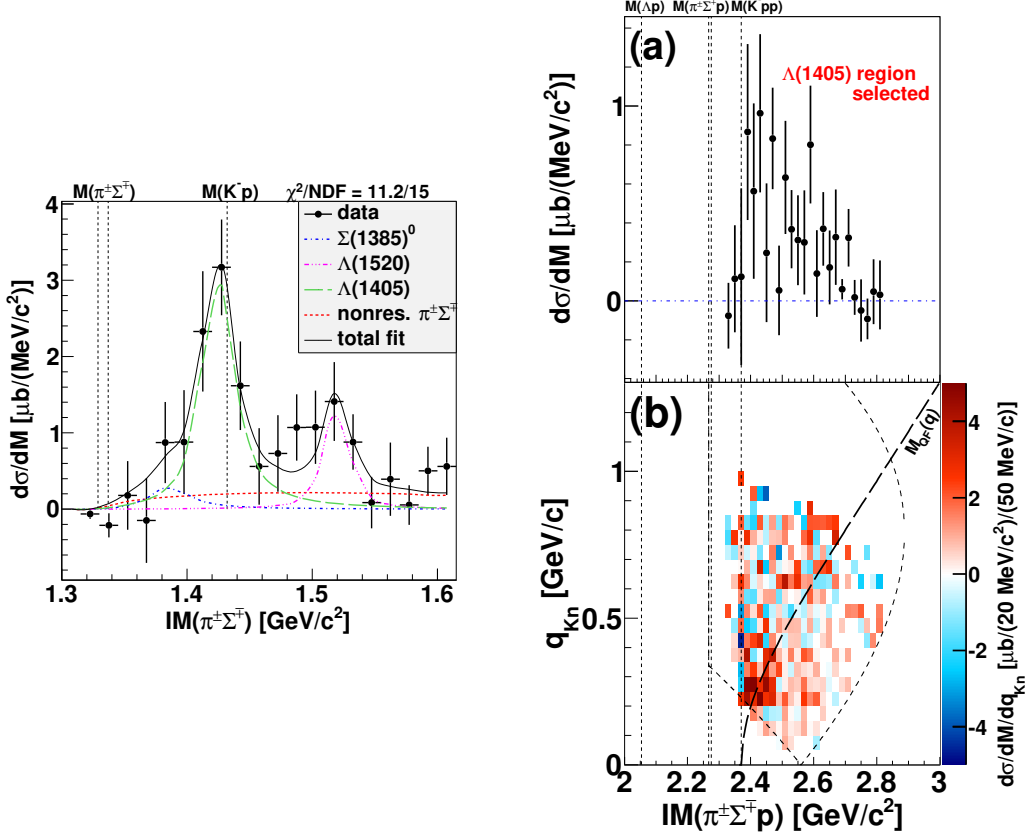
Figure 3: (left) Efficiency and acceptance corrected $\pi^{\pm}\Sigma^{\mp}$ invariant mass in the $\pi^{\pm}\Sigma^{\mp}pn$ final state. The spectrum is fitted with $\Sigma(1385)$, $\Lambda(1405)$, $\Lambda(1520)$ and quasi-free $\pi^{\pm}\Sigma^{\mp}$ background. (right) (a) Efficiency and acceptance corrected $\pi^{\pm}\Sigma^{\mp}p$ invariant mass and (b) q versus $IM(\pi^{\pm}\Sigma^{\mp}p)$ in the $\Lambda(1405)$ region. In (b), the kinematical quasi-free function $M_{QF}(q)$ of $K^{-}N \to \bar{K}n$ followed by $\bar{K}NN \to \Lambda(1405)p$ is also plotted.

region is shown in Fig. 3 (right). One can see that the $\Lambda(1405)pn$ events distribute above the $M(Kpp)$ mass threshold in the $\pi^{\pm}\Sigma^{\mp}p$ invariant-mass spectrum. The curve originating at $M = M(Kpp)$ in Fig. 3 (right)(b) represents the kinematical centroid of the quasi-free absorption process M_{QF}, as with the case of the Λpn final state. The curve reproduces the q-dependence of the event distribution rather well not only in the small q region around 0.3 GeV/c but also in the large q region around 0.7 GeV/c. Therefore the results strongly indicate that the $\Lambda(1405)$ is produced via the quasi-free processes followed by the two-nucleon absorption process.

On the other hand, the structure below the mass threshold can not be seen where we found the "$K^{-}pp$" state in the Λp spectrum. From a theoretical point of view, the $\bar{K}NN$ is a resonant state in the $\bar{K}NN - \pi\Sigma N - \pi\Lambda N$ coupled-channel system, hence the mesonic $\pi\Sigma N$ decays are expected to be dominant compared to the non-mesonic

ΛN decay [38]. However, the experimental result shows quite small $\pi\Sigma N$-decay branch of the "K^-pp" bound state. This discrepancy would be naively interpreted using the decay phase-space volume of the "K^-pp". The $\pi\Sigma N$-decay phase space below the $M(Kpp)$ mass threshold is kinematically limited in the $\pi\Sigma$ decay, while the Λp-decay phase space has no limitation reaching to ~ 300 MeV/c^2 below $M(Kpp)$. Therefore, the decay branches into non-mesonic YN channels can be widely opened when the "K^-pp" bound state is formed. This interpretation is consistent with our observation of the "K^-pp" in the Λp channel; the obtained width of ~ 100 MeV is larger than theoretical expectations based on the mesonic $\pi\Sigma N$ decays.

It can also be interpreted by considering the scattered-kaon energy of the first-step $K^-N \to {}^\cdot\bar{K}{}^\prime n$ process in the laboratory frame (E_K^{lab}) as follows.

- When the scattered-kaon energy is above its intrinsic mass m_K ($E_K^{lab} > m_K$), the '$\bar{K}$'$+NN \to \Lambda(1405)p$ reaction is dominant. The energy-momentum mismatch has to be transferred to the proton, *i.e.*, the "K^-p" bound state as $\Lambda(1405)$ is formed above the $M(Kpp)$ mass threshold.

- On the other hand, when the kaon energy is below the intrinsic mass ($E_K^{lab} < m_K$), the "K^-pp" bound state is formed via the '$\bar{K}$'$+NN \to$ "K^-pp" reaction. The "K^-pp" is produced via $\bar{K}$ capture by two residual nucleons under the energy-momentum match condition below $M(Kpp)$.

Thus, the E15 experiment opened a new era of experimental research on the kaonic nuclei with the virtual kaon beam produced from the in-flight (K^-, N) reactions. This was realized by using the world's highest intensity kaon beam available at J-PARC. However, we found several difficulties to proceed with further investigation of the kaonic nuclei with the existing setup as described in Sec. 3. Therefore, we propose the series of new experiments with the modified K1.8BR beamline and a new large acceptance detector system, to accomplish the systematic research on the light kaonic nuclei.

2　Purpose of the Proposed Experiment

The final physics goal of the experiment we proposed is to investigate $\bar{K}$ meson property in nuclei via the $\bar{K}N$ interaction. The meson-baryon interactions close to the mass thresholds are known to provide crucial information on the interplay between spontaneous and explicit chiral symmetry braking. Among meson-baryon interactions, the $\bar{K}N$ interaction is an important probe to understand this important aspect of low-energy QCD. However, due to the presence of the $\Lambda(1405)$ state located just below the $\bar{K}N$ mass threshold, which is theoretically considered as a quasi-bound state of $\bar{K}N$ today, investigations of the $\bar{K}N$ interaction are very complicated and thus difficult. One of the straightforward methods to reveal the interaction is to precisely measure the line shape of the $\Lambda(1405)$ state with the $\bar{K}N \to \pi\Sigma$ channels, as we demonstrated at the E31 experiment. On the other hand, the possible existence of kaon-nuclear
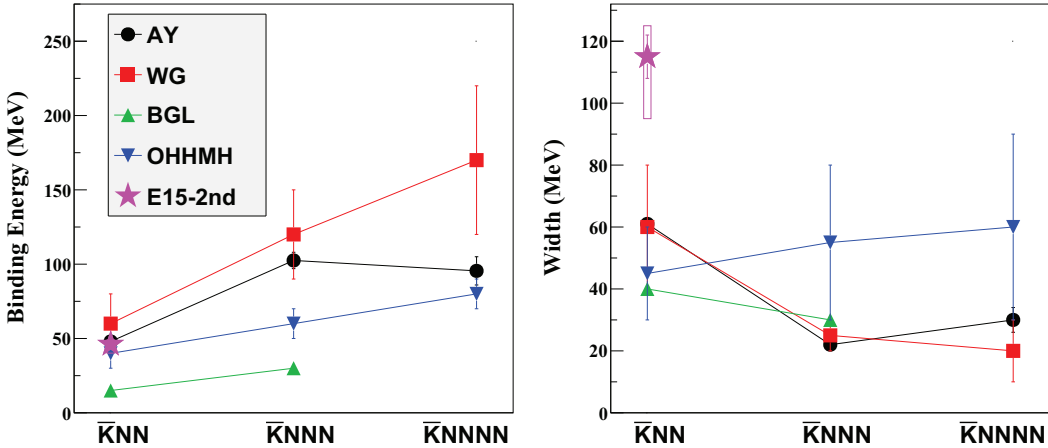
Figure 4: Summary of the theoretical calculation of kaonic nuclear states in light nuclei from $A = 2$ to 4 in different models AY [6, 7], WG [13], BGL [16], and OHHMH [22]. The result obtained at the E15-2nd experiment is also plotted [34].

quasi-bound states has been widely discussed on the analogy of the $\Lambda(1405)$ state. The properties of the kaonic nuclei strongly depend on the $\bar{K}N$ interaction, thus systematic investigation of the kaonic nuclei will also provide the information on the $\bar{K}N$ interaction below the mass threshold.

In the proposed experiment, we focus on an investigation of the kaonic nuclei with the mass number $A = 3$, $\bar{K}NNN$, to derive the strength of the $\bar{K}N$ interaction from the system size dependence of the properties. The property of the kaonic nuclei is mainly characterized by the binding energy and decay width, whose system size dependence is calculated with several theoretical models as summarized in Fig. 4. In the calculations, the expected values are widely spreaded out due to the difference of the $\bar{K}N$ interaction models, but all calculations show that the larger size nuclei have the larger binding energy. The main difference of the models is the $\bar{K}N$ potential below the mass threshold, which has been controversial for a long time. As for the width, the theoretical calculations take into account only mesonic decay channels including $\pi\Sigma$ and $\pi\Lambda$, thus the calculated width would become large if the models adopt non-mesonic decay channels as demonstrated in Ref. [17]. By comparing the obtained properties of the $\bar{K}NNN$ state with those of the previously reported "K^-p" ($=\Lambda(1405)$) and "K^-pp" states, we reveal the $\bar{K}N$ interaction below the $\bar{K}N$ mass threshold.

3 Experimental Method and Apparatus

So far, the $\bar{K}NNN$ state has been searched for with stopped K^- beam mainly. The KEK-PS E471/E549 collaborations measured the inclusive ${}^4\text{He}(K^-_{stopped}, p/n)$ re-
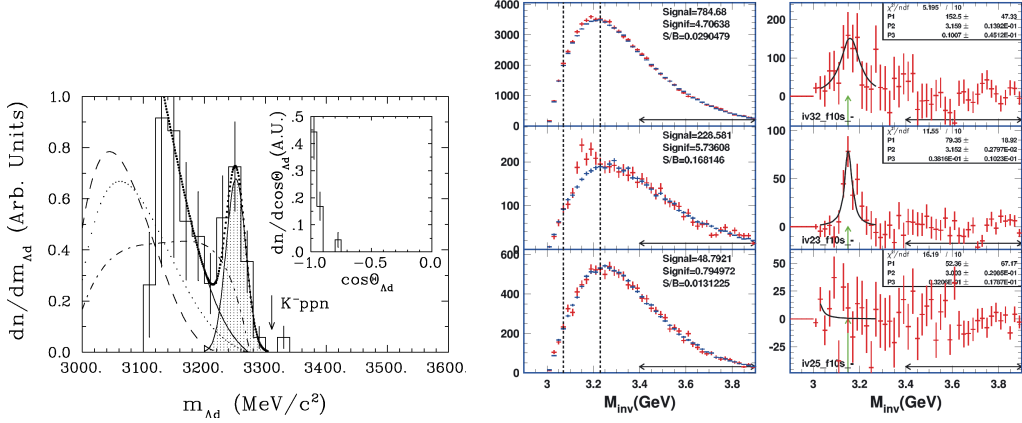
Figure 5: Invariant mass spectra of Λd reported from (left) the FINUDA collaboration in the ${}^{6}\mathrm{Li}(K^-_{\mathrm{stop}}, \Lambda d)3N$ reaction [41] and (right) the FOPI collaboration in the Ni+Ni reaction at 1.93 AGeV [42].

actions with a spectrometer dedicated to TOF measurement of protons and neutrons [39,40]. However, they found no specific peak structures below the mass threshold of $M(\bar{K}NNN)$ in the missing mass spectra from the reactions. This is due to huge backgrounds originated from the two nucleon absorption processes, $\bar{K}NN \to YN$, and quasi-free hyperon productions and its decays, $\bar{K}N \to \pi Y$, whose production mechanisms are quite complicated in the stopped K^- reactions. The backgrounds can not be discriminated kinematically from the signal with small production cross section in the inclusive measurement. This situation is quite similar to the inclusive measurement of ${}^{3}\mathrm{He}(K^-, n)X$ performed in the early analysis stage of the E15 experiment [32]. In the analysis, no significant peak structure was found due to the huge backgrounds from quasi-free processes and the two nucleon absorption processes, however, the "K^-pp" signal was observed by reducing the huge backgrounds with the exclusive measurement of ${}^{3}\mathrm{He}(K^-, \Lambda p)n$; the cross section of the "K^-pp" signal ($\sim 10~\mu\mathrm{b}$) is much smaller than that of the quasi-free processes (~ 10 mb) [33,34].
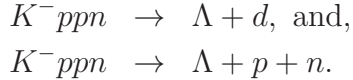
On the other hand, there are two reports of observation of the "K^-ppn" candidates below the mass threshold in the Λd invariant mass spectrum with the stopped K^- reactions (FINUDA) and the heavy-ion collisions (FOPI). The FINUDA collaboration reported that the candidate has the binding energy of ~ 60 MeV and the width of ~ 40 MeV as shown in Fig. 5 (left) [41]. The candidate reported from the FOPI collaboration has much deeper binding energy of ~ 150 MeV with broader width of ~ 100 MeV, as shown in Fig. 5 (right) [42]. However, because these measurements were performed only inclusively, contributions of multi-nucleon absorption process and intermediate states of N^*/Y^* to the peak structure can not be excluded. In addition, those statistics reported were very limited, thus the results still remain speculated as of today.

11

Therefore, the key to the experimental search is to adopt a simple reaction and to measure it exclusively. Simple reactions, such as in-flight $\bar{K}$ induced reactions with light target nuclei, would make the production mechanism clear. Exclusive measurement is also crucial to distinguish a small and broad signal from largely and widely distributed quasi-free and multi-nucleon absorption backgrounds.
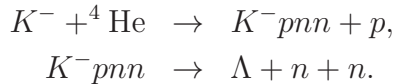
In the proposed experiment, we perform the exclusive measurements of the production and decay of the "K^-ppn" state using

$$K^-_{in-flight} +^4 \mathrm{He} \quad \rightarrow \quad K^-ppn + n$$

reaction followed by expected no-mesonic decays of

$$K^-ppn \quad \rightarrow \quad \Lambda + d, \text{ and,}$$
$$K^-ppn \quad \rightarrow \quad \Lambda + p + n.$$

We determine the binding energy and the width from the invariant mass reconstruction of the decays. The invariant mass is obtained as a function of the momentum transfer to distinguish the bound-state production from the quasi-free processes and multi-nucleon absorption processes by the event kinematics as demonstrated in the E15 analysis. In the same $K^- +^4 \mathrm{He}$ reaction, it can be possible to measure the isospin partner of "K^-ppn", $i.e.$, the "K^-pnn" state via

$$K^- +^4 \mathrm{He} \quad \rightarrow \quad K^-pnn + p,$$
$$K^-pnn \quad \rightarrow \quad \Lambda + n + n.$$

Comparison of the properties between the isospin partners is of special importance to investigate the internal structure of the kaonic nuclei. However, because two neutron detection is required to identify the K^-pnn decay, the measurement is experimentally challenging.

We realize the $\bar{K}NNN$ production using the (K^-, N) reaction at the K1.8BR beamline, as successfully performed in the previous experiment E15; a recoiled virtual kaon ('$\bar{K}$') generated by $K^-N \rightarrow$ '$\bar{K}$' n processes can be directly induced into residual nucleons within the strong interaction range. We utilize 1.0 GeV/c incident kaon to maximize $\bar{K}N$ reaction rate at zero degree as shown in Fig.1. Incoming K^- beam is identified and its momentum is analyzed by the beamline spectrometer. The beam kaon is irradiated to the targets located at the final focus point, and the all particles generated from the reactions are identified with a cylindrical detector system (CDS) that surrounding the target system. The kaonic nuclei are identified via invariant-mass reconstruction of the decay particles. By detecting the nucleon coming from the initial (K^-, N) reactions, or by identifying that with missing mass technique, we realize exclusive measurement of the production of the kaonic nuclei.

With the existing detector system, however, we have found some difficulties to achieve the further systematic investigations as follows:

1. **Available kaon beam**
   In the E15 experiment, we installed a dipole magnet (D5) at just upstream of the final focus point and modified the original design of the K1.8BR beamline optics. This modification was aimed to achieve the forward neutron TOF resolution of $\sim$ 10 MeV/c^2 with 15 m TOF length between a T0 counter and a forward neutron counter array. By this modification, the beamline length became long (~ 3.7 m), which resulted a decrease of available kaon beam.

2. **CDS acceptance**
   The existing CDS consists of a solenoid magnet, a cylindrical wire drift chamber (CDC), and a cylindrical detector hodoscope (CDH) having a solid angle coverage of 59%. To determine the isospin and parity of the kaonic nuclei, in general, one need to investigate the production and decay topology with 4π acceptance. In the "K^-pp" case of E15, we attempted to measure the decay asymmetry of the Λp decay and Λ decay itself, however, we found the hardness of the measurement due to acceptance hole caused by lack of the acceptance in the forward and backward directions.

3. **Neutron detection with the CDS**
   In the $\Lambda(1405)pn$ analysis with the ^{3}He$(K^-, \pi^\pm\Sigma^\mp p)n$ measurement described in Sec. 1, we have suffered from huge backgrounds mainly originated from neutron misidentification. This is due to poor neutron detection efficiency and background particles generated from reactions between charged/neutral particles and the solenoid-magnet yoke. We have also found that the poor neutron efficiency makes difficult to investigate the "K^-pn" state – the isospin partner of "K^-pp" which is expected to decay into Λn channel. Thus, neutron detection with the CDS becomes more important for the systematic measurements of the kaonic nuclei, because we need to detect decay neutrons from the exotic states with large mass (neutron) number and to reconstruct its invariant mass.

To overcome such difficulties, we are planing to conduct an upgrade of the K1.8BR spectrometer. We construct a new large cylindrical detector system (CDS) having $\sim 4\pi$ acceptance with capability of neutral particle detection, and modify the K1.8BR beamline by shortening the beam length. The CDS upgrade enables us to measure the various expected decay modes, *i.e.* not only non-mesonic decay channels but also mesonic decay channels of the kaonic nuclei. Furthermore, detection of γ from the Σ^0 decay with an electromagnetic calorimeter is desirable. The beamline modification makes it possible to use more large beam intensity under the same MR beam power.

The details of each apparatus used for the experimental programs, including the existing system, are described in the following sub-sections.
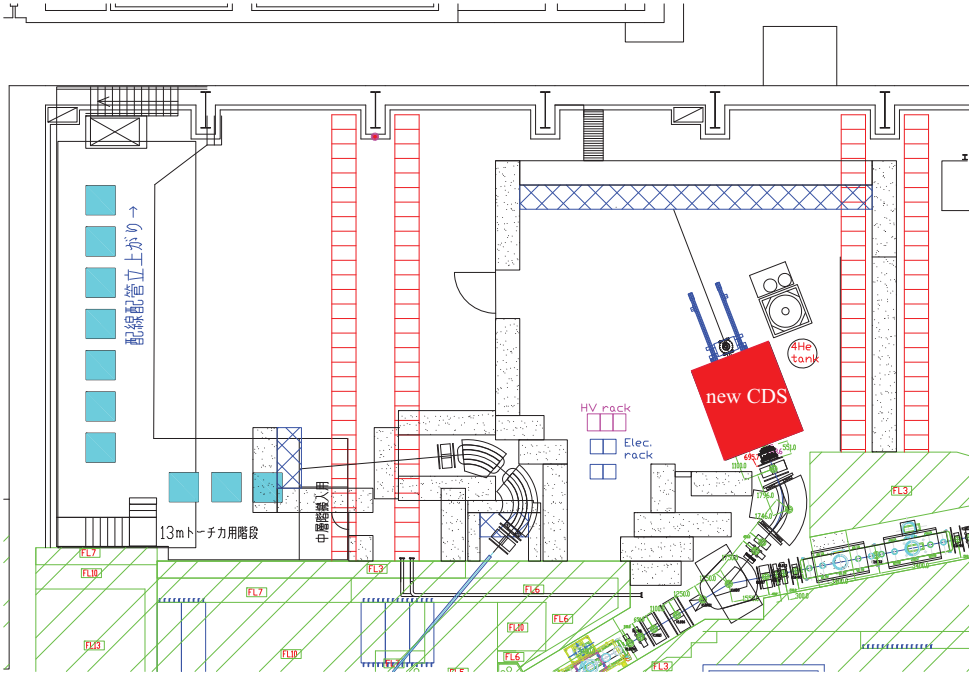
Figure 6: Plan of the rearrangement of the K1.8BR experimental area. The new CDS is also shown as a colored box in the beamline.

3.1 Beamline Spectrometer

We propse to modify the existing beamline of the K1.8BR which was constructed to be dedicated to the (K^-, N) measurements with forward neutron and proton counter arrays. In the modification, we remove the most downstream dipole magnet of D5 so that the available beam yield is maximized. Since the beam trajectory is drastically changed by the removal, the beam dump is also required to be moved along the beam direction. Therefore, we rearrange the K1.8BR experimental area as shown in Fig. 6. At the modified experimental area, the beam dump is moved from the west side of the hadron hall currently installed to the north side.

Figure 7 shows the calculated beam optics with the modified setup. The shortening of the beamline (~ 3.7 m) is essential for experiments using the low momentum kaon beam. It should be noted that, because the size of the CDS becomes larger than the previously used CDS as described in Sec. 3.3, the final focusing point is shifted to the downstream of the beamline by ~ 1.2 m, *i.e.*, the shortening length is effectively ~ 2.5 m. Beam focus might also be improved by this modification, however, we adopt a conservative value of the fiducial-volume-selection efficiency of 0.65: the value was obtained at the predecessor experiments in which the same target cell was used as the proposed experiment. This is because the beam size at the final focus point strongly depends on beamline tuning, which is hardly reproduced by the simulation codes of
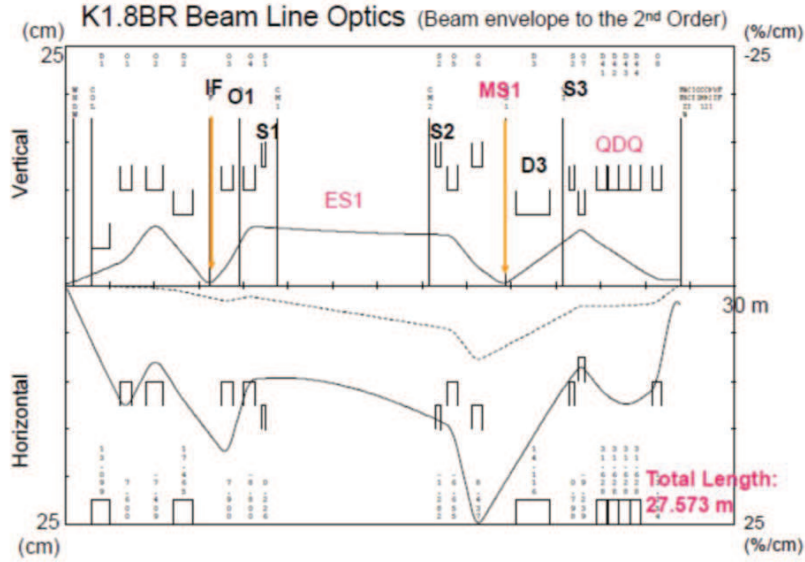
図8 : K1.8BR ビームエンベロープ

Figure 7: Beamline optics of the modified K1.8BR beamline.

TRANSPORT and TURTLE, even though for the existing beamline of the K1.8BR. Thus, the available kaons on target are conservatively estimated to increase ~ 1.4 times, which corresponds to 3.2×10^5 kaons on target per spill at the beam power of 90 kW with 5.2 s repetition cycle [†].

The beamline spectrometer is composed of beamline magnets, trigger counters, beam trackers, and a kaon identification counter [43,44]. The beam TOF measurement is performed with a newly developed beam hodoscope tracker (BHT) installed at the just upstream of the D4 magnet and a T0 counter after D4. Kaon beams are identified with an aerogel Cherenkov counter whose reflective index is 1.05. The kaon beam is tracked with the BHT and a beamline chamber, and the momentum of the beam is analyzed with this tracking information together with the beam optics of the D4 magnet. The expected momentum resolution is 2×10^{-3}, which was the same resolution achieved at the predecessor experiments with the D5 magnet. We also use a beam definition counter (DEF) installed just upstream of the target cell to suppress the trigger rate. We can use the existing apparatus at the current K1.8BR beamline except for the BHT; we plan to construct the BHT using an array of thin plastic scintillator slab $(3 \sim 5[W] \times 3[T] \times 150[H]$ mm$)$ with MPPC readout.

[†]2.0×10^5 (Run85, 2020 @ 51kW) $\times 0.65$ (fiducial volume selection) $\times$ 1.4 (beamline length) $\times$ 90/51 (beam power) $\sim 3.2 \times 10^5$.
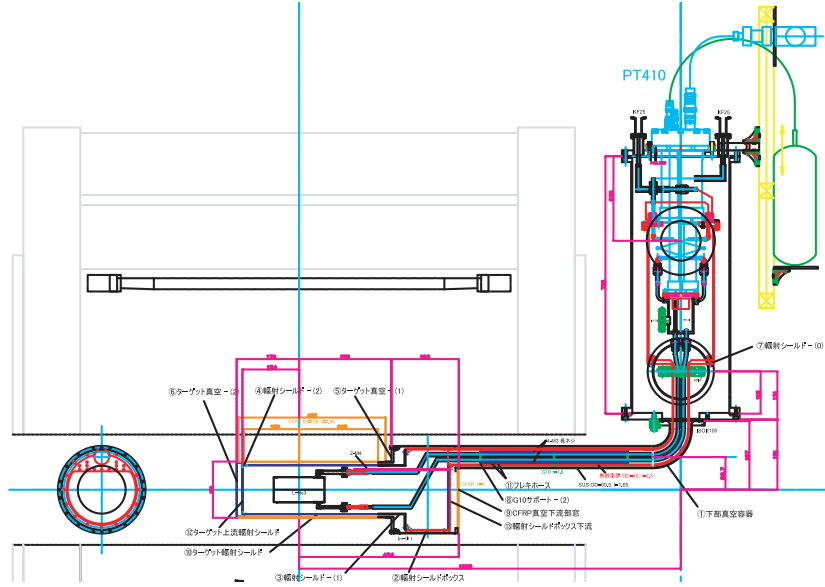
Figure 8: Schematic view of the target system at the K1.8BR beamline. The figure shows the setup for the P73 experiment, but we modify the system dedicated to the proposed experiment by changing a transfer chamber located between a main cryogenic chamber and a target chamber.

3.2   Target System

Targets used in the proposed experiment are liquid ^{4}He target. In the proposed experiment, we use a newly developed pulse tube refrigerator system for the hyper triton measurement (J-PARC P73 experiment) which can liquefy all types of $H_2/D_2/^3He/^4He$ gases with the same system. To achieve a high cooling power below 3 K, we use a pulse tube refrigerator PT410 manufactured by CRYOMECH. The new system for the P73 experimental setup has been successfully operated at the K1.8BR beamline. The achievable temperature of the system is 2.7 K, in which the density of the liquid ^{4}He is 0.144 g/cm^3 with a stability of better than 0.1%. A pure beryllium target cell developed for E15 is used, whose dimension is 6.8 cm in diameter and 13.7 cm in length.

3.3   Cylindrical Detector System (CDS)

Efficient and high precision reconstruction of decay particles from the target region with large acceptance is a key for the proposed experiment. To this end, we newly construct a large size CDS to be replaced with the previously used CDS at the K1.8BR beamline. The requirements for the new CDS are as follows:

4π **acceptance**

The exclusive measurement of the (K^-, N) reactions is essential for the experiment. To detect particles involved in the reaction as much as possible, the detector acceptance needs to be substantially identical to 4π, for both of charged and neutral particles coming from the target region. The large acceptance system can reduce backgrounds attributed to particle misidentification from missing particles.

High resolution

The spacial and timing resolution of the the detector system has to be as good as possible to precisely reconstruct the decays of the kaonic nuclei and to determine its properties. At minimum, the resolution achieved with the previously used CDS is required for the new CDS to efficiently reconstruct the $\Lambda \to \pi^- p$, $\Sigma^\pm \to \pi^\pm n$, and $K^0 \to \pi^+ \pi^-$ decays.

Neutral-particle detection

Detection of neutral particles from the production and decay is of special importance in the proposed experiment. Especially, large detection efficiency for neutron is a key in the series of the experimental programs. In reconstruction of the sequential decay of $\Lambda(1405) \to \pi^\pm \Sigma^\mp$ followed by $\Sigma^\pm \to \pi^\pm n$, the decay neutron has low momentum of a few 100 MeV/c. Thus we have to measure the neutron with time-of-flight technique using a plastic scintillator which is the best way of the low-momentum neutron measurement. A electromagnetic calorimeter is also an essential apparatus to measure the $\Sigma^0 \to \gamma\Lambda$ decay, $e.g.$, pure $I = 0$ channel of the $\Lambda(1405) \to \pi^0 \Sigma^0$ is the most important channel to deduce the spectral shape of the $\Lambda(1405)$.

To fulfill the requirements described above, the new CDS is designed to be composed of five main components: a superconducting solenoid magnet, a cylindrical drift chamber (CDC), backward and forward drift chambers (BDCs/FDCs), a neutron counter (NC), and an electromagnetic calorimeter (ECAL). A conceptual design of the new CDS is shown in Figs. 9 and 10. The size of the new CDS is much larger than that of the existing CDS whose size is indicated as blue boxes in Figs. 9. Design of each detector component is described in the following subsections.

Noted that the component of the CDS would be easily rearranged to be dedicated to individual experimental aims. For instance, to measure the polarization of the decay Λ and proton from the "$K^- pp$" state for the spin determination, we are planing to install a polarimeter consisted of thin plastic scintillators and a tracker system by replacing the NC (and the ECAL). Details of "the $K^- pp$ project" will be shown in the other proposal in the near future. The installation of such tracker system also enables us to perform high precision measurement of charged decay modes of the kaonic nuclei with a few MeV/c^2 mass resolution, thanks to large lever arm length of the tracking volume.
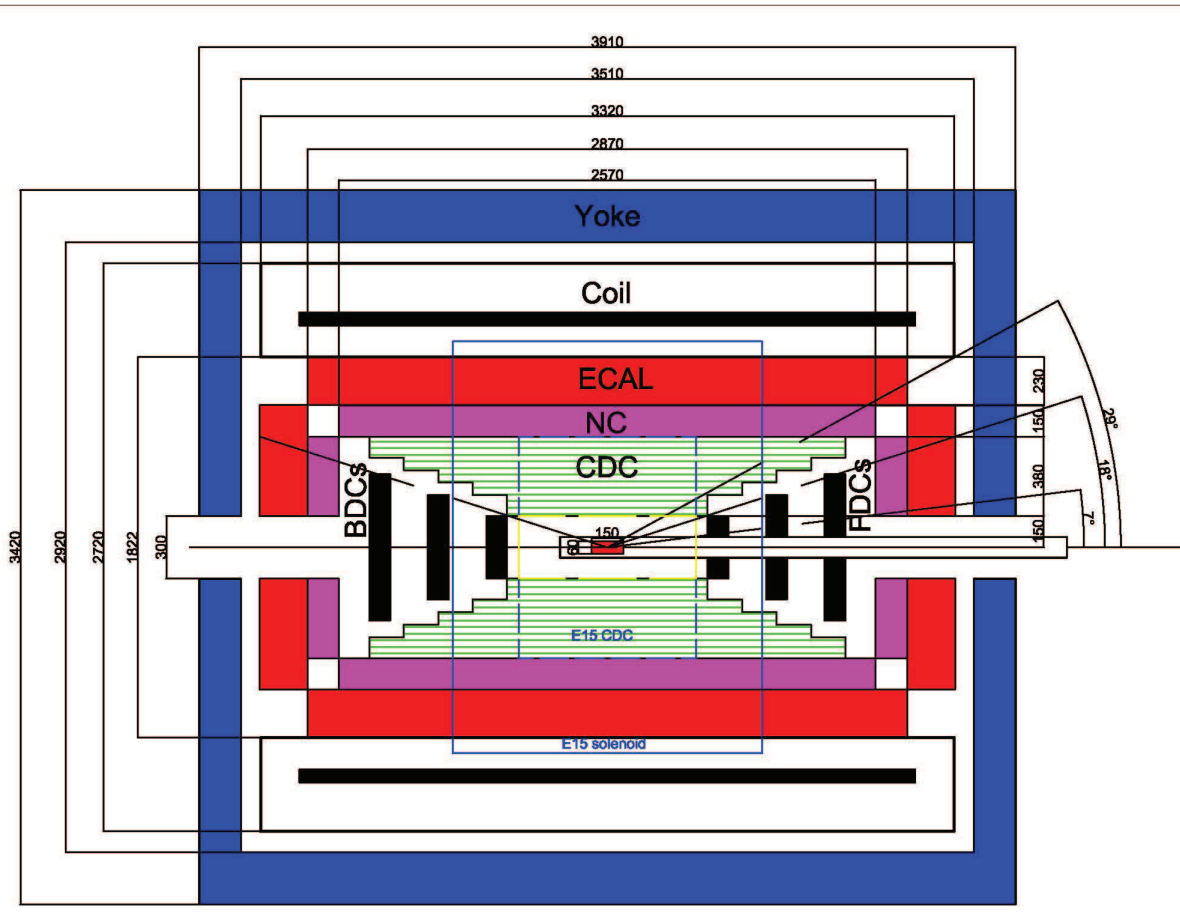
Figure 9: Conceptual design of the new CDS (cross section).

3.3.1 Superconducting Solenoid Magnet

The spectrometer magnet of the CDS is a solenoidal type. In the proposed experimental programs, we adopt almost the same design of 'the detector solenoid magnet' of the COMET experiment developed by the KEK Cryogenic Science Center. The magnet provides a uniform field strength inside the tracking volume whose strength we use is 0.7 T at the center of the magnet [‡].

The magnet uses the Ni-Ti-Cu superconductor with three GM refrigerators, and is operated with a 80 kVA power supply (AC415V - 200A). The bore diameter of the magnet is 1.8 m and length is 3.3 m with an overall weight of $\sim$ 25 tons. The shape of the return yoke is square shape whose external dimensions is 3.4 m $\times$ 3.4 m $\times$ 3.9 m.

[‡]The solenoid magnet is designed to be able to provide the magnetic field of 1.0 T for the COMET experiment.
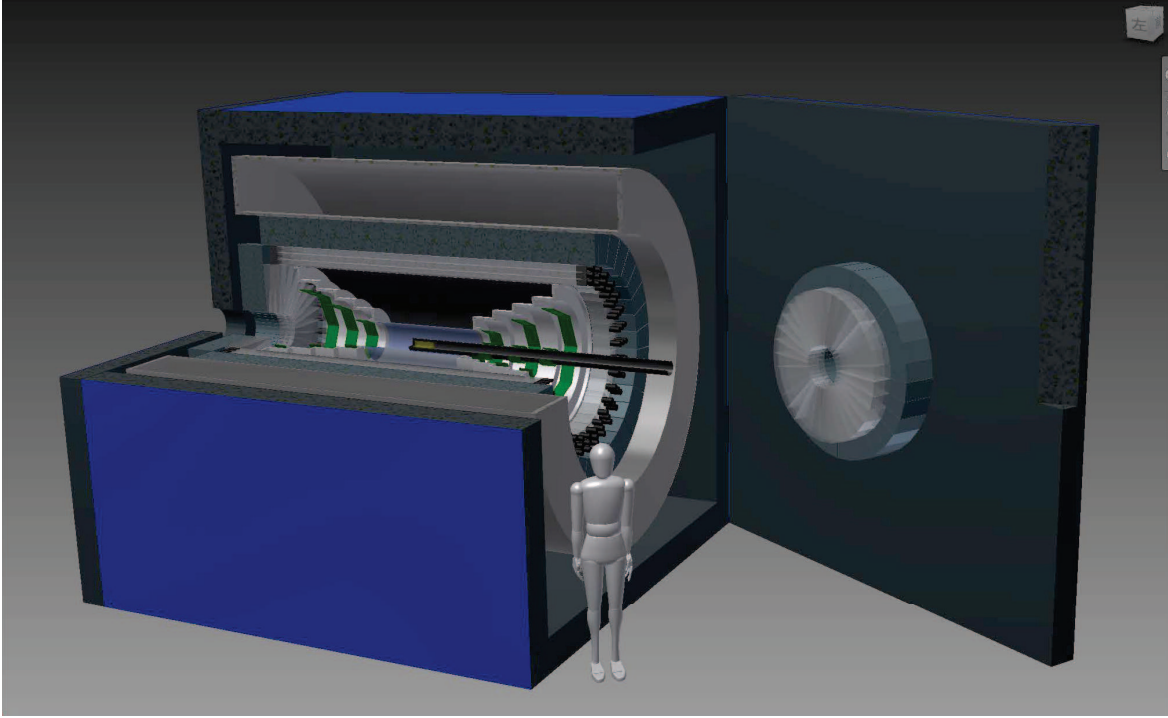
Figure 10: Conceptual design of the new CDS (3D model).

3.3.2 Cylindrical Drift Chamber (CDC)

The CDC is a cylindrical wire drift chamber that contains 17 layers of anode wires. The conceptual design of the CDC is shown in Fig. 11, which is symmetric in the z direction (beam direction) to provide a $29° < \theta < 151°$ angular coverage. The CDC has conical-shaped end-plates to maximize the forward and background acceptance where is covered by the FDCs, the BDCs, and the PID counters. The outer radius is 530 mm and the inner radius is 150 mm, with the longest wire length of 2.2 m. To obtain a good tracking efficiency for low-p_t tracks, the CDC is designed without the inner wall, but a CFRP cylinder is used as the outer wall.

The CDC has 17 layers of small hexagonal cells with a typical drift length of 9 mm, which are grouped into 7 super-layers. Table 1 gives the conceptual parameters of the wire configuration, which are based on those of the previously used CDC. The 8 stereo layers tilted by about 3.5° are used to obtain longitudinal position information. The number of readout channels is ~ 2150.

We plan to use gold-plated tungsten of 30 μm ϕ for the sense wires and gold-plated aluminum of 100 μm ϕ for the field and guard wires, which are supported by feedthroughs with a bushing inserted at the end. The drift gas is 1 atm of mixed argon (50%) - ethane (50%). A high voltage is applied to the field and guard wires, and the sense wires are kept at ground potential. As the readout electronics, we use
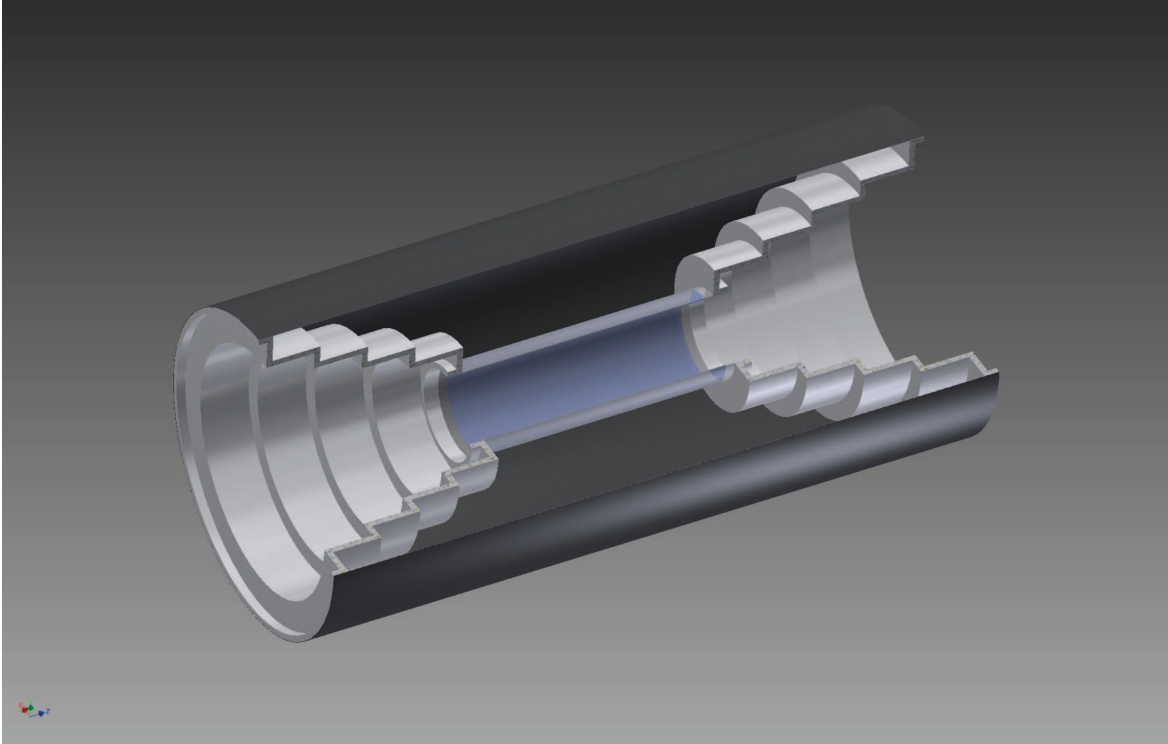
Figure 11: Conceptual design of the new CDC).

the previously used CDC readout system, *i.e.*, a preamp card with ASDs (SONY-CXA3653Q, $\tau = 16$ ns) and Hadron Universal Logic (HUL) boards. The expected performance of the CDC is almost the same as that of the existing CDC used for the predecessor experiments; the transversed momentum resolution of 5.3 % $p_t \oplus$ 0.5 %/β corresponding to $\sim 3\%$ on 500 MeV/c particles.

3.3.3 Vertex Fiber Tracker (VFT)

The high-resolution vertex determination is indispensable to discriminate between the signals and backgrounds with event topology such as distance of closest approach method: for instance, the $\pi^\pm \Sigma^\mp \rightarrow \pi^+ \pi^- n$ decays would be separated clearly together with the invariant mass and decay vertex topology. With only the CDC, the vertex resolution of the beam direction (z-direction) is expected to be ~ 1 cm, although that of the radius direction (r-direction) is a few mm. This is due to small tilt angles of the stereo layers which is limited by the feedthrough layout. By introducing the VFT, the vertex resolution in the beam direction will be improved to a few mm with a combination of the CDC tracking information.

The VFT is installed on the outer wall of the target chamber ($r \sim 80$ mm), which consists of 4 layers of scintillating fibers of 1 mm ϕ having $UU'VV'$ configuration. In

20

Super layer	Layer	Wire direction	Radius (mm)	Cell width (degree)	Cell width (mm)	Stereo angle (degree)	Signal channel per layer
A1	1, 2, 3	X, X' X	190 - 230	5.00	~ 18.0	0	72
U1	4, 5	U, U'	250 - 300	3.60	~ 18.5	~ ± 3.5	100
V1	6, 7	V, V'					
A2	8, 9, 10	X, X' X	320 - 360	3.00	~ 18.0	0	120
U2	11, 12	U, U'	380 - 430	2.25	~ 17.0	~ ± 3.5	160
V2	13, 14	V, V'					
A3	15, 16, 17	X, X' X	450 - 490	2.00	~ 16.5	0	180

Table 1: Conceptual parameters of the wire configuration of the CDC.

the U and V layers, the fibers are tilted by ± 45 degrees. For readout, the system developed for the fiber-tracker system in the E50 experiment will be used. The total readout channel is ~ 2000 ($=\sim 500 \times 4$).

3.3.4 Backward and Forward Drift Chambers (BDCs/FDCs)

The BPCs and FDCs are respectively installed just upstream and downstream of the target aiming to reconstruct backward- and forward-going particles cannot be detected by the CDC. Each chamber is a set of octagonal planar wire drift chambers, which is composed of 3 modules with different size depending on the distance from the target.

The BPCs are placed 0.5 m, 0.8 m, and 1.1m upstream from the target with the size of 30 cm, 50 cm, 70 cm inscribed circle diameters, respectively. Each chamber consists of 8 layers with an XX'YY'XX'YY' configuration, whose layer contains 32, 64, 96 sense wires with a drift length of ~ 4 mm, respectively. The FDCs are placed 0.5 m, 0.8 m, and 1.1m downstream from the final focus, and are almost the same structure as the BPCs but the centers of the chambers is cut out not to interfere with the target chamber. The chamber gas is an argon (80%) - isobutane (20%) mixture, and we use the same readout electronics as the CDC, *i.e.*, the ASD preamp cards and the HUL boards.

3.3.5 Charged-particle Hit Counter (CHC)

In the proposed experimental programs, the neutral particle detections is a key of the systematic studies of the kaonic nuclei. To realize the efficient data accumulation of both charged and neutral particles, online counting of the both charged- and neutral-particle multiplicity is essential. For this purpose, we install a thin segmented plastic scintillation counter as the CHC for the trigger counter. The charged-particle multiplicity is obtained with the CHC, while the neutral-particle multiplicity is obtained with the combination of the CHC-veto and NC/ECAL information.

The CHC is divided into a cylindrical barrel part (barrel CHC) and the two facing endcap sections (endcap CHCs), which is located at just front of the NC. Each of the barrel and endcap CHCs has a thickness of 3 mm whose scintillation light is read out

using wave-length shifting fibers and MPPCs. Segmentation of the CHC is the same as that of the NC and ECAL as described below.

3.3.6 Neutron Counter (NC)

The NC is an array of segmented plastic scintillation counters used for the neutron detection. The first layer of the NC is also used for the charged-particle identification as a hodoscope counter. The NC is divided into a cylindrical barrel part (barrel NC) and the two facing endcap sections (endcap NCs). Each of the barrel and endcap NCs has a thickness of 15 cm divided into three layers. The expected neutron detection efficiency is 15% $\sim$ 45% which depends on the neutron momentum.

The barrel NC is located at a radius of 530 mm from the beam axis covering a polar angle range from 29 to 151 degrees. The barrel NC consists of 32 modules in a layer whose scintillators are made of Eljen EJ-200 with dimensions of 2.6 m in length, $\sim$ 120 mm in width, and 50 mm in thickness. The scintillation light is transferred through light guides to a pair of Hamamatsu R7761 fine-mesh 19-dynode photomultipliers 1.5 inches in diameter.

The endcap NCs are mounted on the each endcap of the solenoid magnet together with a endcap ECAL described in the next subsection, which cover a polar angle range from 7(160) to 20(173) degrees. The endcap NCs consist of 32 trapezoid modules in a layer whose scintillators are made of Eljen EJ-200 with dimensions of 400 mm in length, 30 -100 mm in width, and 50 mm in thickness. We plan to use MPPC arrays to read out the scintillation light from the both sides of the module, by assembling 4 $\sim$ 10 pieces of 6 mm $\times$ 6 mm MPPCs.

3.3.7 Electromagnetic Calorimeter (ECAL)

The ECAL is a sampling-type calorimeter used for photon energy measurement. The ECAL is divided into a cylindrical barrel part (barrel ECAL) and the two facing endcap sections (endcap ECALs). Each of the barrel and endcap ECALs has a thickness of 23 cm. We plan to construct the ECAL with a lead - scintillating-fiber calorimeter developed for the KLOE experiment [45] or a lead - scintillator-slab with wave-length shifting fibers calorimeter used in such as the CLAS experiment [46]. In each case, $\sim$ 15 radiation length is required to precisely reconstruct the photon energy with $\Delta E/E \sim 6\%/\sqrt{E(GeV)}$.

The barrel ECAL is located at a radius of 680 mm from the beam axis covering a polar angle range from 32 to 148 degrees. The barrel ECAL consists of 32 modules with dimensions of 2.9 m in length, 130 - 170 mm in width. The endcap ECALs are mounted on the each endcap of the solenoid magnet together with a endcap NC, which cover a polar angle range from 7(158) to 22(173) degrees. The endcap ECALs consist of 32 trapezoid modules with dimensions of 500 mm in length, 30 -130 mm in width.
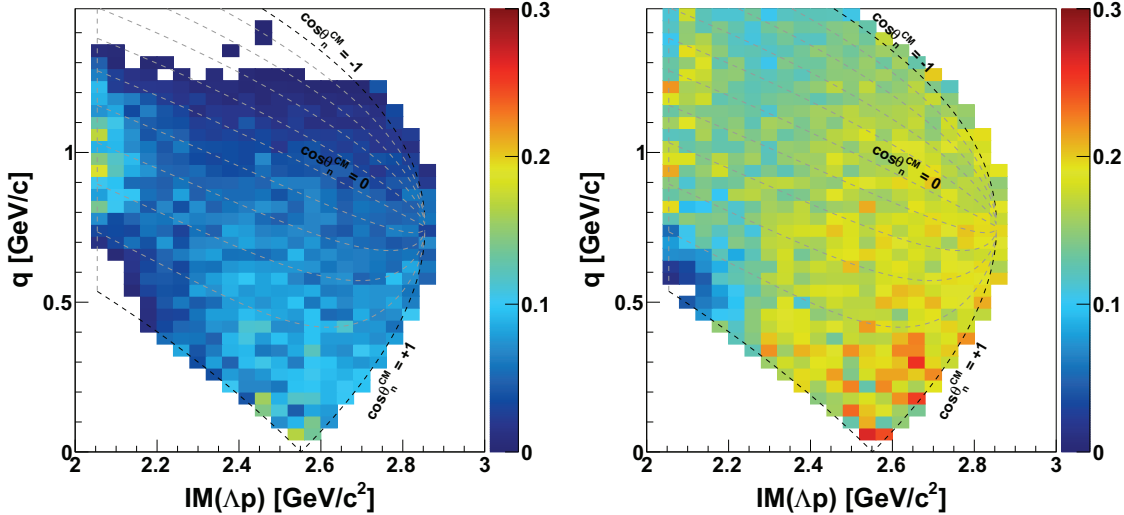
Figure 12: Detector acceptance for the Λp detection with the CDS in the $K^- + {}^3\text{He}$ $\rightarrow \Lambda pn$ reaction. The left figure shows the acceptance with the existing CDS (E15-CDS), and the right shows that with the newly constructed CDS (new-CDS). The relation between q and $\cos(\theta_n^{CM})$ is also represented, where $\cos(\theta_n^{CM})$ denotes the polar angle of the missing neutron in the center-of-mass frame of the $K^- + {}^3\text{He}$ reactions.

3.3.8 Acceptance

Figure 12 shows a comparison of the detector acceptance between the existing CDS (E15-CDS) and the newly constructed CDS (new-CDS) for the $K^- + {}^3\text{He} \rightarrow \Lambda pn$ final state which has been well studied in the E15 experiment. The figure shows the acceptances for the Λp detection with the CDS in the $q - IM(\Lambda p)$ plane. The acceptances are evaluated with a full Monte-Carlo simulation whose details are described in Sec. 4. The detector acceptance of the new CDS is drastically improved as clearly seen in the figure. The enlargement of the acceptance is quite essential for the proposed experiments to efficiently detect particles in the final state and to specify the reaction channel in unambiguous manner.

3.4 Trigger

A dedicated hardware trigger is developed to meet experimental requirements. The kaon beam trigger is constructed with the same procedure as the previously performed experiments at the K1.8BR beamline. The elementary beam trigger is constructed by coincidence signals from the beamline counters, and the kaon beam trigger is selected from the beam trigger by using the kaon identification counter (*i.e.*, the aerogel Cherenkov counter).

To select an event associated with the kaonic nuclei production, we use the simplest charged-multiplicity trigger implemented in hardware level with the CHC. The number of the CHC hits (CHC_n) is selected according to the target species. For example, CHC_3 is used for the K^- ^{4}He $\to$ "K^-ppn" $n \to \Lambda d \to \pi^- pd$, where three charged particles detection is required. In addition, we introduce the neutral-multiplicity trigger to select neutron and/or γ-ray in online level. We implement the neutral trigger using a FPGA logic board of the HUL, with the CHC and the NC/ECAL hit information. The CHC is used as a veto counter for neutral particles, and the neutral trigger is constructed by taking coincidence between the veto-CHC and NC/ECAL hits in the same ϕ-direction.

By combining the charged- and neutral-multiplicity triggers, we can realize any dedicated trigger for from the $\bar{K}N$ to $\bar{K}NNNN$ measurements. We use the the Hadron DAQ system with the HUL as the online data acquisition system, whose maximum accumulation rate has been confirmed to reach to ~ 10 k events per spill with more than 90% DAQ efficiency. In the proposed experiment, the expected trigger rate of the main trigger (for example of "K^-ppn" – main trigger is CHC_3) is a few kHz by taking into account the previous experiments. Therefore, trigger rate is controllable according to the physics purpose by using the combination of the charged- and neutral-multiplicity triggers.

4   Yield Estimation and Expected Spectrum

4.1   Yield Estimation

In the $K^- + {}^3$He $\to \Lambda pn$ measurement, we obtained the production cross section of the "K^-pp" as $\sigma_{Kpp}^{tot} \cdot BR(\Lambda p) \sim 10$ μb [34]. To estimate the expected yield of the "K^-ppn", we assume that the "K^-ppn" cross section in the $K^- + {}^4$He $\to X + n$ reaction is the same of the "K^-pp" $\to \Lambda p$, i.e.,

$$\sigma_{Kppn}^{tot} \cdot BR(\Lambda d) \quad \sim \quad 10\mu\text{b},$$
$$\sigma_{Kppn}^{tot} \cdot BR(\Lambda pn) \quad \sim \quad 10\mu\text{b}.$$

The detector acceptance of the CDS (Ω_{CDS}) is evaluated with a full detector simulation by assuming the obtained event distributions in E15. For the simulation, the GEANT4 toolkit ver.10.2.3 with the "QGSP_BERT_HP" physics list [47] is used. The momentum dependence of the neutron-detection efficiency with the NC is also simulated with the GEANT4 physics process.

---

*In the E15 experiment, we used the siphon-type refrigerator system, where 1.30 K operation was realized – density of liquid ^{3}He is 0.081 g/cm^3. During the operation of the refrigerator system, we needed ^{4}He refrigerant refill work for 1 hour everyday. Now we use the new target system with the pulse tube refrigerator system which does not need ^{4}He refrigerant. On the other hand, because achievable temperature is bit high of 2.7 K (density of 0.070 g/cm^3) with the new system, the available number of target is decreased. As for the ^{4}He liquefaction used in this proposed experiment, the available

Table 2: Estimated yields normalized by 1 G (10^9) K^- beam, for typical expected decay modes. The binding energies of ~ 50 MeV and widths of ~ 100 MeV are assumed for each bound state.

	K^-pp (^{3}He)		K^-pn (^{3}He)	K^-ppn (^{4}He)	K^-ppn (^{4}He)
decay mode	Λp		Λn	Λd	Λpn
$\sigma^{tot} \cdot BR$	10 μb		assumed to be 10 μb		
N_{beam}	10^9				
spectrometer	E15-CDS		new-CDS		
N_{target}	1.92×10^{23} *		1.73×10^{23} *	2.58×10^{23}	
ϵ_{beam}	0.55				
ϵ_{DAQ}	0.74		0.9		
$\epsilon_{trigger}$	0.93				
$\epsilon_{fiducial}$	0.65				
Ω_{CDS}	0.12	0.28	0.085	0.27	0.077
ϵ_{CDS}	0.6		0.3	0.6	0.3
N	33	120	18	170	25

The estimated yields for each channel normalized by 1 G (10^9) K^- beam are summarized in Tab. 2, where those for the "K^-pp" and "K^-pn" states are also shown as a reference. We assume the similar spectrum shape of the observed "K^-pp" in E15 for each bound state, with the binding energies of ~ 50 MeV and widths of ~ 100 MeV. The CDS acceptance of Ω_{CDS} is obtained for the exclusive reconstruction of $^{3/4}$He$(K^-, \Lambda p/\Lambda n/\Lambda d/\Lambda pn)N$ where the missing N is identified from the missing mass. The yields are calculated using the following equation:

$$N = \sigma \times N_{beam} \times N_{target} \times \epsilon,$$
$$\epsilon = \epsilon_{DAQ} \times \epsilon_{trigger} \times \epsilon_{beam} \times \epsilon_{fiducial} \times \Omega_{CDS} \times \epsilon_{CDS},$$

where

$$
\begin{aligned}
N &: \text{ expected yield,} \\
\sigma &: \text{ cross section including the branching ratio,} \\
N_{beam} &: \text{ number of the beam kaons,} \\
N_{target} &: \text{ number of the target particles,} \\
\epsilon &: \text{ total experimental efficiency,} \\
\epsilon_{DAQ} &: \text{ DAQ efficiency,} \\
\epsilon_{trigger} &: \text{ trigger efficiency,}
\end{aligned}
$$

number of target is not changed because the target density is almost the same between 1.30 K and 2.7 K.

Table 3: Estimated yields under the MR beam power of ~ 90 kW with 5.2 s repetition cycle. In the list of the E15-2nd experiment, we show the results of Run#65 conducted in 2015, whose obtained yield is almost consistent with the calculated yield with the E15-2nd condition.

	K^-pp (^{3}He)	K^-pn (^{3}He)	K^-ppn (^{4}He)	K^-ppn (^{4}He)
decay mode	Λp	Λn	Λd	Λpn
$\sigma^{tot} \cdot BR$	10 μb	assumed to be 10 μb		
experiment	E15-2nd	exp. in near future	proposed exp.	
MR beam power	42 kW	90 kW		
beam-time duration	1 month	3 weeks		
accelerator up-time	0.89	0.9		
# of K^- beam	62×10^9	155×10^9		
# of K^- on target	40×10^9	100×10^9		
# of expected yield	1.7×10^3	13×10^3 2.0×10^3	19×10^3	2.8×10^3

$$
\begin{aligned}
\epsilon_{beam} \quad &: \quad \text{analysis efficiency of the beam kaons,} \\
\epsilon_{fiducial} \quad &: \quad \text{efficiency of fiducial volume selection,} \\
\Omega_{CDS} \quad &: \quad \text{detector acceptance of the CDS,} \\
\epsilon_{CDS} \quad &: \quad \text{analysis efficiency of the CDS.}
\end{aligned}
$$

In the calculation of N_{target}, fiducial volume length of 11.8 cm is adopted, which was set to the E15-2nd analysis. We assume the same parameters obtained and evaluated in the analysis of the predecessor experiments at the K1.8BR: $\epsilon_{beam} = 0.55$, $\epsilon_{trigger} = 0.93$, $\epsilon_{fiducial} = 0.65$, $\epsilon_{CDS} = 0.6$ for $\Lambda p/\Lambda d$ channels, and $\epsilon_{CDS} = 0.3$ for $\Lambda n/\Lambda pn$ channels whose decay neutron is detected with the NC of the CDS (or the CDH of the E15-CDS).

At the modified K1.8BR beamline, we expect the kaons on target of 3.2×10^5 per spill with the momentum of 1.0 GeV/c, under the MR beam power of ~ 90 kW with 5.2 s repetition cycle. Table 3 show the estimated yields with 3 weeks beam time under assumption of 90% accelerator up-time – 100 G kaons on target (155 G beam kaon without fiducial volume selection). Compared to the obtained "K^-pp" yield at the E15-2nd, we expect ~ 10 times larger statistics of "K^-ppn" $\rightarrow \Lambda d$ accumulation, and, the same statistical order of the "K^-ppn" $\rightarrow \Lambda pn$.

4.2 Expected Spectrum

Figure 13 shows the expected spectra of the K^- ^{4}He $\rightarrow \Lambda dn$ and the Λpnn final states with 155 G kaon beam (100 G kaons on target) corresponding to 3 weeks data
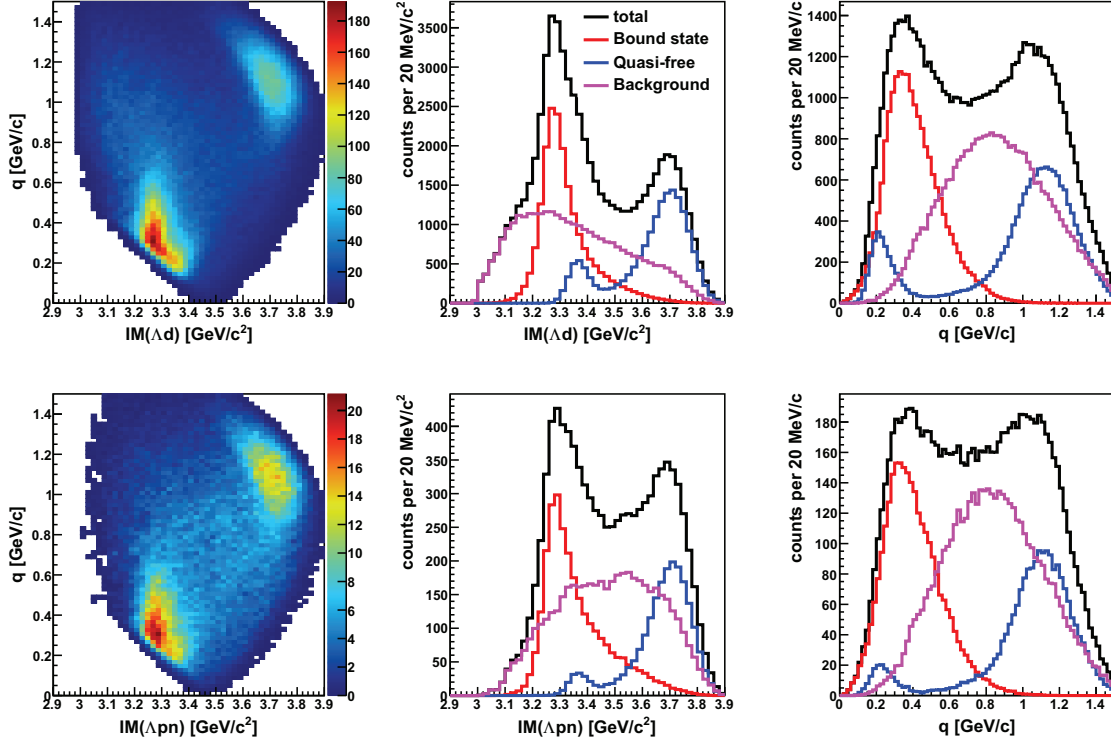
Figure 13: Expected spectra of the (top) Λd and (bottom) Λpn in the $K^- + {}^4\text{He} \to \Lambda d + n$ and $\Lambda pn + n$ final state with 155 G kaon beam (100 G kaons on target), respectively. Here, we assume the cross section of the $K^- ppn$, quasi-free, and background of 10 μb, 10 μb, and 20 μb, respectively, based on the E15 results.

taking under 90 kW beam power. For the $K^- ppn$ state in the figures, we assume the similar distribution of the "$K^- pp$" observed in E15: the binding energy of ~ 50 MeV, the width of ~ 100 MeV, and the Gaussian form factor of ~ 400 MeV/c with 10 μb ($\sigma \cdot BR$). As for the quasi-free process and the broad background, we also used the similar parameters obtained in the $K^- + {}^3\text{He} \to \Lambda pn$ final state in E15.

The spectra for each process are generated using the Geant4 simulation, in which we assume the same resolution of the existing CDS to reconstruct the simulated tracks – $5.3\% \times p_t \oplus 0.5\%$ for charged particles and $\sim 10\% \times p \oplus 7\%$ for a neutron. In the assumed conditions, the bound states are clearly identified not only in the invariant mass spectra but also in the $q - IM$ distribution, which is the most important feature of the proposed experiment. By investigating the specific structures in the $q - IM$ distribution, we can kinematically identify the signal of the bound state. Figure 14 shows a demonstration of the signal enhancement by selecting the momentum transfer of $0.3 < q < 0.6$ GeV/c. In the region, we expect that the bound state is clearly separated from the quasi-free process, as we shown in Fig. 2 using the E15 data of Λpn

27
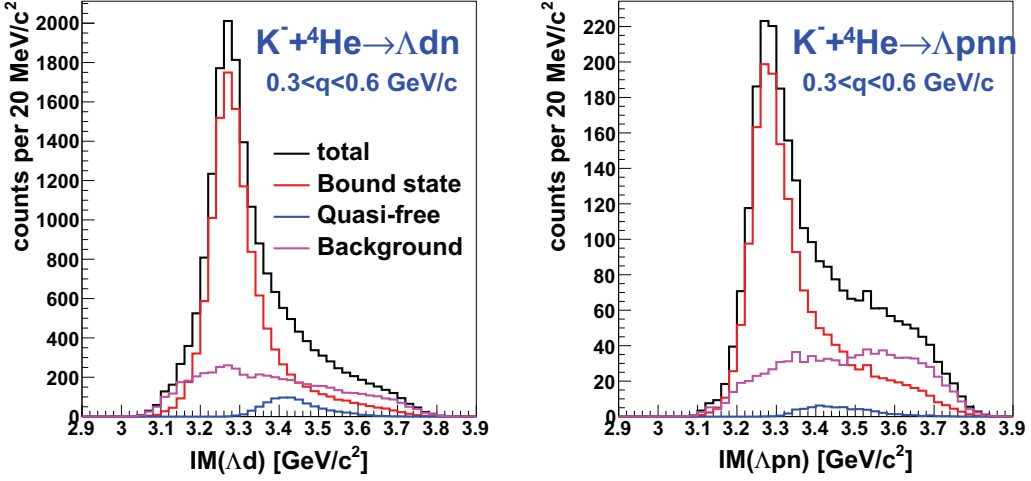
Figure 14: Expected invariant mass spectra of the (left) Λd and (light) Λpn in the region of $0.3 < q < 0.6$ GeV/c, which are obtained from Fig. 13.

final state.

It should be noted that if the K^-ppn state forms the dense and compact state as expected, its decay branch including a deuteron might be small because a deuteron has a loosely bound structure. In reactions of stopping K^- in ^{4}He target, there might be some hints of the branching fraction although the reaction is different from the kaonic nuclei decays. In the reactions, the fraction between Σ^-pd and Σ^-ppn is known to be almost the same [48]. By analogy with this result, we adopt a positive assumption in the proposal that the branching ratio of the Λd decay from the K^-ppn state would be the same as that of the Λpn decay. In any case, the lower limit we can identify the $K^-ppn \rightarrow \Lambda d$ decay as it is would be $\sim \mu$b in the proposed experiment, if the cross sections of the backgrounds are the same as assumed in Fig. 13. On the other hand, the Λpn decay branch should be large regardless of the Λd decay, thus the measurement with the newly constructed CDS having neutron detection capability is essential for the systematic study of the kaonic nuclei.

5 Schedule and Beam Time Plan

Figure 15 shows the time line of the preparation for the proposed experiment. We would like to perform the proposed experiment in 2023, thus the detector system required for the experiment has to be ready in 2022. The modification of the K1.8BR experimental area is hopefully conducted in the summer of 2021, whose cost is expected to be covered by KEK budget. The design works of the main part of the CDS, *i.e.* the super-conducting solenoid, the CDC, and the NC, are going on and will be completed

	2020			2021				2022				2023				2024			
	Q2	Q3	Q4	Q1	Q2	Q3	Q4	Q1	Q2	Q3	Q4	Q1	Q2	Q3	Q4	Q1	Q2	Q3	Q4
Magnet	design	purchase (S.C. wires)		construction			test and commisioning			integration		comm. run		physics run				analysis, publication	
VFT		design		construction			test and commisioning			integration		comm. run		physics run				analysis, publication	
CDC		design		construction			test and commisioning			integration		comm. run		physics run				analysis, publication	
Backward DC		design		design and construction				test and comm.		integration		comm. run		physics run				analysis, publication	
Forward DC		design		design and construction				test and comm.		integration		comm. run		physics run				analysis, publication	
Chamber Readout		design		R&D		production		test and comm.		integration		comm. run		physics run				analysis, publication	
BHT		design		construction		test and commisioning				integration		comm. run		physics run				analysis, publication	
CHC		design		construction		test and commisioning				integration		comm. run		physics run				analysis, publication	
NC	design	purchase		assembly			test and commisioning			integration		comm. run		physics run				analysis, publication	

Figure 15: Schedule of the preparation for the proposed experiment.

in 2020. Then the construction of the main part will be conducted in 2021, and after the detector test and commissioning those system will be integrated at J-PARC in 2022. The backward and forward drift chambers will be also designed and constructed by the middle of 2022. After commissioning of the whole detector system with cosmic ray in the middle of 2022, the experiment will be ready in the beginning of 2023.

Table 4 show a summary of the requested beam time. At around 2023, the MR beam power will increase by ~ 90 kW. We expect the negative-kaon beam yield of ~ 320 k per spill with the momentum of 1.0 GeV$/c$ at the K1.8BR beamline. In the beam time plan, we do the detector commissioning with actual kaon beam for one week as a beginning, where we optimize the detector operation under the same condition of the production run. After completion of the commissioning, we continue the performance study run with the liquid H_2 target for one week to confirm detector performance by demonstrating $K^0 \to \pi^+\pi^-$, $\Lambda \to \pi^- p$ and $\Sigma^\pm \to \pi^\pm n$ reconstruction with the CDS. The one week data taking corresponds to ~ 50 G K^- beam which is ~ 10 times larger than that accumulated in the E15 H_2 run in 2015. Then the production run with liquid ^{4}He target is carried out for three weeks. We expect ~ 155 G K^- beam (100 G kaons on target) with the 80% machine up-time, which is ~ 2.5 times larger than that accumulated in the E15 ^{3}He run in 2015.

Table 4: Summary of the beam-time plan.

Duration at 90 kW	K^- beam yield (K^- on target)	Experimental target	Purpose of the experiment
1 week	–	–	commissioning
1 week	50 G (33 G)	Liquid H_2	performance study
3 weeks	155 G (100 G)	Liquid ^{4}He	$\bar{K}NNN$ production

6 Cost Estimation

The cost to construct the new system is summarized in Tab. 5, which will be mainly covered by "the budget of Grand-In-Aid for Specially Promoted Research by MEXT" and RIKEN internal budget. The cost includes constructions of the super-conducting solenoid magnet, the VFT, the CDC, the BDCs and FDCs, the NCs, the CHC, the BHT, and those read-out systems. Fine-mesh PMTs of the previously used cylindrical hodoscope (CDH) are recycled as a part of the read-out of the barrel NC. The ECAL system is expected to be constructed by the international collaborators in the INFN-LNF and SMI with their construction know-how of the KLOE system. If we construct the ECAL from scratch, the estimated cost is reached to ~ 700 M JPY in the case of the KLOE type calorimeter. Therefore we are planing to install the ECAL in the 2nd stage of the experimental programs at the K1.8BR beamline, after enough R&D using a prototype module.

References

[1] M. Iwasaki *et al. Phys. Rev. Lett.* **78** (1997) 3067.

[2] G. Beer *et al. Phys. Rev. Lett.* **94** (2005) 212302.

[3] M. Bazzi *et al. Phys. Lett.* **B704** (2011) 113.

[4] A. D. Martin *Nucl. Phys.* **B179** (1981) 33.

[5] Y. Nogami *Phys. Lett.* **7** (1963) 288.

[6] Y. Akaishi and T. Yamazaki *Phys. Rev.* **C65** (2002) 044005.

[7] T. Yamazaki and Y. Akaishi *Phys. Lett.* **B535** (2002) 70.

[8] N. V. Shevchenko, A. Gal, and J. Mares *Phys. Rev. Lett.* **98** (2007) 082301.

[9] N. V. Shevchenko, A. Gal, J. Mares, and J. Revai *Phys. Rev.* **C76** (2007) 044004.

Table 5: Cost estimation to construct the new system.

Item	Cost [JPY]	Budget Source
Super-conducting Solenoid Magnet	200 M	Grant-In-Aid
VFT	20 M	Grant-In-Aid
CDC	130 M	Grant-In-Aid
Read-out system for CDC	30 M	Grant-In-Aid
Backward DCs	30 M	RIKEN int. budget / Grant-In-Aid
Forward DCs	30 M	RIKEN int. budget / Grant-In-Aid
Read-out system for DCs	20 M	RIKEN int. budget / Grant-In-Aid
BHT	10 M	RIKEN int. budget / Grant-In-Aid
CHC	10 M	RIKEN int. budget / Grant-In-Aid
Scintillator for Barrel NC	30 M	Grant-In-Aid
PMTs for Barrel NC	20 M	Grant-In-Aid
Scintillator for Endcap NC	15 M	Grant-In-Aid
Read-out system for MPPCs	10 M	Grant-In-Aid
Total	$\sim$ 600 M	

[10] Y. Ikeda and T. Sato *Phys. Rev.* **C76** (2007) 035203.

[11] A. Doté, T. Hyodo, and W. Weise *Nucl. Phys.* **A804** (2008) 197.

[12] Y. Ikeda and T. Sato *Phys. Rev.* **C79** (2009) 035201.

[13] S. Wycech and A. M. Green *Phys. Rev.* **C79** (2009) 014001.

[14] A. Doté, T. Hyodo, and W. Weise *Phys. Rev.* **C79** (2009) 014003.

[15] Y. Ikeda, H. Kamano, and T. Sato *Prog. Theor. Phys.* **124** (2010) 533.

[16] N. Barnea, A. Gal, and E. Z. Liverts *Phys. Lett.* **B712** (2012) 132.

[17] M. Bayar and E. Oset *Phys. Rev.* **C88** (2013) 044003.

[18] S. Maeda, Y. Akaishi, and T. Yamazaki *Proc. Jpn. Acad.* **B89** (2013) 418.

[19] J. Révai and N. V. Shevchenko *Phys. Rev.* **C90** (2014) 034004.

[20] A. Doté, T. Inoue, and T. Myo *Prog. Theor. Exp. Phys.* **2015** (2015) 043D02.

[21] T. Sekihara, E. Oset, and A. Ramos *Prog. Theor. Exp. Phys.* **2016** (2016) 123D03.

[22] S. Ohnishi *et al. Phys. Rev.* **C95** (2017) 065202.

[23] A. Doté, T. Inoue, and T. Myo *Phys. Rev.* **C95** (2017) 062201.

[24] A. Doté, T. Inoue, and T. Myo *Phys. Lett.* **B784** (2018) 405.

[25] M. Agnello *et al. Phys. Rev. Lett.* **94** (2005) 212303.

[26] T. Yamazaki *et al. Phys. Rev. Lett.* **104** (2010) 132502.

[27] Y. Ichikawa *et al. Prog. Theor. Exp. Phys.* **2015** (2015) 021D01.

[28] O. Vzquez Doce *et al. Phys. Lett.* **B758** (2016) 134.

[29] R. Del Grande *et al. Eur. Phys. J.* **C79** (2019) 190.

[30] G. Agakishiev *et al. Phys. Lett.* **B742** (2015) 242.

[31] A. O. Tokiyasu *et al. Phys. Lett.* **B728** (2014) 616.

[32] T. Hashimoto *et al. Prog. Theor. Exp. Phys.* **2015** (2015) 061D01.

[33] Y. Sada *et al. Prog. Theor. Exp. Phys.* **2016** (2016) 051D01.

[34] S. Ajimura *et al. Phys. Lett.* **B789** (2019) 620.

[35] T. Kishimoto *Phys. Rev. Lett.* **83** (1999) 4701.

[36] J. M. M. Hall *et al. Phys. Rev. Lett.* **114** (2015) 132002.

[37] T. Yamazaki and Y. Akaishi *Phys. Rev.* **C76** (2007) 045201.

[38] S. Ohnishi, Y. Ikeda, H. Kamano, and T. Sato *Phys. Rev.* **C88** (2013) 025204.

[39] M. Sato *et al. Phys. Lett. B* **659** (2008) 107.

[40] H. Yim *et al. Phys. Lett. B* **688** (2010) 43.

[41] M. Agnello *et al. Phys. Lett. B* **654** (2007) 80.

[42] N. Herrmann *et al. Proc. EXA05 Conference* **ISBN 3-7001-3616-1** (2005) 73.

[43] K. Agari *et al. Prog. Theor. Exp. Phys.* **2012** (2012) 02B009.

[44] K. Agari *et al. Prog. Theor. Exp. Phys.* **2012** (2012) 02B011.

[45] M. Adinolfi *et al. Nucl. Instrum. Meth.* **A482** (2002) 364.

[46] M. Amarian *et al. Nucl. Instrum. Meth.* **A460** (2001) 239.

[47] J. Allison *et al. Nucl. Instrum. Meth.* **A835** (2016) 186.

[48] P. Katz *et al. Phys. Rev. D* **1** (1970) 1267.